

# Hyperbolic times in Minkowski space

Anıl Zenginöglü

Institute for Physical Science and Technology,  
University of Maryland, College Park, MD 20742, USA

## Abstract

Time functions with asymptotically hyperbolic geometry play an increasingly important role in many areas of relativity, from computing black-hole perturbations to analyzing wave equations. Despite their significance, many of their properties remain underexplored. In this expository article, I discuss hyperbolic time functions by considering the hyperbola as the relativistic analog of a circle in two-dimensional Minkowski space and argue that suitably defined hyperboloidal coordinates are as natural in Lorentzian manifolds as spherical coordinates are in Riemannian manifolds. The presence of the null cone adds new elements to this analogy, particularly regarding the smooth foliation of the asymptotic boundary.

## 1 Hyperbolic geometry in relativity

The discovery of hyperbolic geometry is one of the most impactful developments in the history of mathematics. Its revelation by Gauss, Bolyai, and Lobachevsky in the 19th century was the culmination of a story spanning over 2,000 years that rivals any multi-generational science fiction saga in drama and excitement [1, 2]. The subsequent analysis of non-Euclidean geometry by Beltrami, Poincaré, and Riemann was the necessary mathematical development that prepared the ground for special and general relativity as physical theories of space, time, and gravity. Minkowski was keenly aware of the central role that hyperbolic geometry played when he declared the unification of space and time into spacetime as a four-dimensional manifold with a metric of negative signature [3, 4, 5, 6].

The interpretation of Lorentz transformations as hyperbolic rotations gives a visually appealing and intuitive demonstration of relativistic phenomena such as velocity addition or Thomas precession [7, 8, 9, 10]. Hyperbolic geometry not only provides the kinematic space of special relativity [3, 11], it also serves as a model for space that connects a source of radiation to an idealized, far-away observer (see Sec. 3.2).

General time functions that share the asymptotic properties of hyperbolas are called hyperboloidal [12]. The behavior of such hypersurfaces makes them appealing to describe global aspects of spacetimes, including asymptotic boundaries, black hole horizons, and cosmological horizons. In suitable hyperboloidal coordinates, space flows toward null horizons similarly as in the river model of black holes [13, 14]. Hyperboloidal time functions play an increasingly important role in relativity across many active research areas such as black-hole perturbation theory, gravitational waves, and the mathematical analysis of wave equations [15, 16, 17, 18, 19, 20, 21, 22, 23, 24].

In this expository article, I present various aspects of hyperbolic time functions in the simple case of two-dimensional Minkowski space at a level suitable for an advanced course on special relativity. The main objectives are to demonstrate the essential properties of such surfaces and to clarify misconceptions. Most of the discussion requires no more than a basic understanding of Minkowski space and coordinate transformations, but it is still sufficiently general to cover advanced topics. The calculations apply to black holes, cosmological horizons, and null infinity when we treat the space coordinate as the analog of the tortoise coordinate (see Sec. 5.3).

Our discussion starts in Sec. 2 with a quick introduction to Minkowski space and its compactification using Penrose coordinates—an essential tool for understanding the global causal structure of spacetimes. We consider the standard coordinates and their weaknesses in the context of the global causal structure of Minkowski space: the standard time coordinate in Minkowski space is degenerate at infinity. Time functions that respect time translation symmetry must approach null infinity to resolve the asymptotic coordinate singularity.

In Sec. 3, we introduce spacelike hyperbolas as analogs of circles in Euclidean space. We clarify their global causal properties (3.1), demonstrate their necessity for far-away observers (3.2), and present a variational principle underlying their construction as solutions to the isoperimetric problem in Minkowski space (3.3).

Section 4 compares Milne time (4.1) and hyperbolic foliation (4.2), revealing that the analogy between the circle and the hyperbola is not helpful when constructing smooth time functions describing the asymptotic domain. The impact of the asymptotic coordinate singularity in Milne time is demonstrated in a simple wave equation. Global energy is conserved in standard time and Milne time but decays due to radiation to infinity in hyperbolic foliation (4.3).

In Sec. 5, we generalize hyperbolic time functions to hyperboloidal time functions. First, we generalize from one spatial dimension to higher spatial dimensions: from hyperbola to hyperboloids (5.1). Then, we generalize to hyperboloidal time functions that share the relevant asymptotic properties of hyperboloids near null infinity (5.2). We discuss different choices of spatial compactifications in 5.3, which allows us to further clarify the meaning of the terms asymptotically null and hyperboloidal. Whether a surface is asymptotically null or spacelike depends on the spacetime compactification. Finally, we recognize that Penrose coordinates are hyperboloidal arising from a combination of Milne time and hyperbolic foliation (5.4). Much of this discussion is relevant in the context of black holes and cosmological horizons when the space coordinate is treated as the tortoise coordinate.

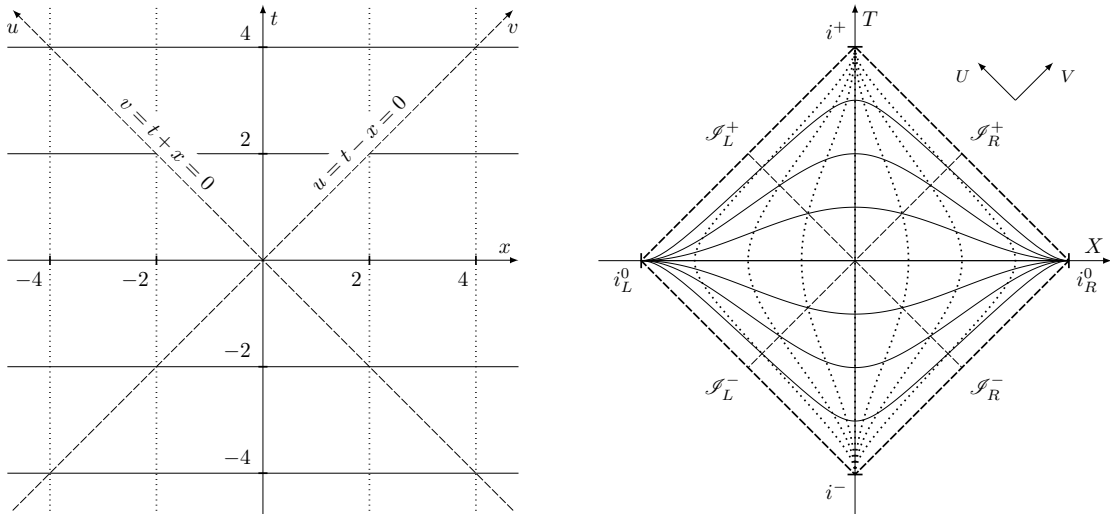


Figure 1: The left panel shows the standard Minkowski coordinate grid in  $\{t, x\}$  and the null cone through the origin representing the axes of null coordinates  $\{u, v\}$ . The right panel shows the level sets of standard coordinates in a Penrose diagram  $\{T, X\}$ . Solid, horizontal lines represent spacelike curves, dotted, vertical lines represent timelike curves, and dashed lines represent null curves in all figures. Slices of the standard time coordinate  $t$  intersect at spatial infinities, suggesting that the time coordinate  $t$  is unsuitable for the global structure.

## 2 The standard time coordinate in Minkowski space

Our stage is the two-dimensional Minkowski space. The Minkowski metric in standard coordinates  $t \in (-\infty, \infty)$  and  $x \in (-\infty, \infty)$  in natural units is

$$ds^2 = -dt^2 + dx^2. \quad (1)$$

The negative signature in the metric gives rise to the null structure consisting of left- and right-going null rays:  $v = t + x$ ,  $u = t - x$ . A coordinate grid in Minkowski space is depicted in Fig. 1 along with the null cone through the origin,  $t \pm x = 0$ , representing the axes of null coordinates  $\{u, v\}$ . Solid, horizontal lines represent spacelike curves, dotted, vertical lines represent timelike curves, and dashed lines represent null curves.

The global causal structure of Minkowski space is represented in a Penrose diagram: a conformal diagram using Penrose coordinates  $\{T, X\}$ . The general idea is conformal compactification, which maps the infinite Minkowski space to a finite space with a boundary representing infinity [25, 26]. Many such mappings are available, as we will review in Sec. 5.3. The historical choice by Penrose is the tangent function applied to the null coordinates. Specifically, we introduce coordinates  $U = \arctan u$  and  $V = \arctan v$  which map the infinite interval  $(-\infty, \infty)$  to the finite, open interval  $(-\pi/2, \pi/2)$ . Squeezing infinite distances to a finite range leads to a singular metric at the limiting points

$$ds^2 = -du dv = - \left( \frac{1}{\cos U \cos V} \right)^2 dU dV. \quad (2)$$

We capture this singular behavior in a coordinate-dependent scale factor called the conformal factor  $\Omega = \cos U \cos V$ . Considering the conformally rescaled, regular metric  $\bar{d}s^2 = \Omega^2 ds^2$ , we add the limiting points of the open interval to our domain and obtain the compact interval  $[-\pi/2, \pi/2]$ , completing the conformal compactification.

One typically introduces time and space coordinates  $T = (U + V)/2$  and  $X = (V - U)/2$  with the range  $|T| + |X| \in [-\pi/2, \pi/2]$ . The Penrose diagram on the right panel of Fig. 1 is drawn in these coordinates. The conformal boundary is the zero set of the conformal factor given by  $|U| = |V| = \pi/2$ , or  $|T| + |X| = \pi/2$ . This boundary is not part of Minkowski space but represents the asymptotic limit of its geodesics. In particular, spacelike geodesics end at spatial infinity,  $i_{\{R,L\}}^0 = \{T = 0, X = \pm\pi/2\}$ ; timelike geodesics end at timelike infinity,  $i^\pm = \{T = \pm\pi/2, X = 0\}$ ; and null geodesics end at null infinity denoted by  $\mathcal{I}_{\{R,L\}}^\pm$ . Null infinity is also called scri for the ‘‘script I’’ symbol  $\mathcal{I}$  used to denote it.

The main advantage of conformal compactification is that it replaces asymptotic limits such as  $x \rightarrow \infty$  or  $u \rightarrow \infty$  with local analysis at the boundary. Penrose coordinates perform this compactification along the null coordinates so that null rays are straight lines at 45 degrees. The Penrose diagram of Minkowski space is discussed in most textbooks on relativity, and Fig. 1 is familiar to most practitioners [27, 28, 29, 30]. An advanced discussion of conformal methods in general relativity can be found in the monograph [31].

Penrose coordinates for time  $T$  and space  $X$  are not direct compactifications of the standard coordinates  $t$  and  $x$ . There is an intermediary step involving null directions. It is instructive to see why direct compactification does not work. Setting  $t = \tan \bar{t}$  and  $x = \tan \bar{x}$ , we get

$$ds^2 = -\frac{d\bar{t}^2}{\cos^4 \bar{t}} + \frac{d\bar{x}^2}{\cos^4 \bar{x}}.$$

One cannot capture the singularity of this metric at the boundary  $|\bar{t}| = |\bar{x}| = \pi/2$  in a conformal factor. The underlying geometric reason is that the standard coordinates are singular at their asymptotic endpoints,  $i_{R,L}^0$  and  $i^\pm$ , where they intersect. This problem affects any effort to construct a time foliation that asymptotes to spatial infinity and respects time symmetry. We discuss the case of spatial infinity below as we are primarily interested in time functions, but similar arguments also apply to the timelike infinities,  $i^\pm$ . In Sec. 5.4, we will see that Penrose coordinates are direct compactifications of coordinates with hyperbolic geometry and are, therefore, hyperboloidal.

### **The standard time coordinate is singular at spatial infinity.**

Level sets of  $t$  intersect at the spatial infinities,  $i_{\{R,L\}}^0$ , as seen on the Penrose diagram in Fig. 1. This intersection is reminiscent of radial rays in polar coordinates and indicates that the time coordinate  $t$  is unsuitable for the global causal structure.

Looking at the left panel of Fig. 1, students find it hard to believe that the  $t$  slices are singular at infinity. However, any coordinate system will look like a Cartesian grid when plotted with respect to itself. We can see the singular behavior only when we compare the coordinates to another, more suitable system. This is true for standard coordinates of Minkowski space as it is for polar coordinates of Euclidean space.

The reason for the coordinate singularity at spatial infinity is the vanishing of the timelike Killing field,  $\partial_t$ . Expressing the timelike Killing field in Penrose coordinates, we get

$$\partial_t = \cos^2 U \partial_U + \cos^2 V \partial_V = (1 + \cos(2T) \cos(2X)) \partial_T - \sin(2T) \sin(2X) \partial_X. \quad (3)$$

The norm of the timelike Killing field with respect to the conformally regular metric is the conformal factor,  $\|\partial_t\|_{\Omega^2 ds^2} = \Omega$ . The norm vanishes at the conformal boundary, indicating that the timelike Killing field becomes null at infinity. At spatial and timelike infinities, however, all vector field components in (3) vanish. These points are fixpoints of the timelike Killing field causing the intersection of time slices. One cannot have a regular time coordinate that approaches spatial infinity and preserves the time-translation symmetry.

A similar problem appears at the Killing horizons of stationary spacetimes (the bifurcation sphere in Schwarzschild time, the origin of Minkowski space in Rindler time, or the cosmological horizon of de Sitter space in static time). There is a long history of confusion and misconception about the nature of these singularities, especially for black holes [32, 33, 34, 35]. The fact that such a coordinate singularity already appears for the global structure of Minkowski space was not recognized until Penrose revealed this structure in the 1960s. Null coordinates resolve this asymptotic coordinate singularity by foliating the conformal boundary. We will see an alternative resolution with spacelike surfaces in Sec. 4.

### **The standard time coordinate is not operationally meaningful at spatial infinity.**

The level sets of  $t$  represent space for globally synchronized inertial observers at rest relative to each other. This notion of “now” as a snapshot in time has been abstracted from our everyday experience with weak gravitational fields, slow speeds, and small distances. Its construction requires the synchronization of clocks based on mirrors and is, therefore, operationally meaningful only in the vicinity of an inertial observer. However, as an observer moves farther from a source, one cannot construct such a global time function operationally. For example, astrophysical sources of gravitational radiation are typically thousands or millions of light years away, so synchronization of clocks would take many thousands or millions of years. We cannot synchronize our time function with such sources. Asymptotic observers have only access to the null rays that reach them from the source.

In the next sections, we will see that spacelike hyperbolas resolve these problems.

## **3 Spacelike hyperbola**

In a historical talk during the eightieth meeting of the Assembly of Natural Scientists and Physicians in Cologne in 1908, Minkowski presented the unification of space and time into spacetime [5, 6]. He demonstrated the invariance of his new metric under Lorentz transformations using the unit hyperbola  $t^2 - x^2 = 1$ . The hyperbola plays a fundamental role in Minkowski space as the set of points equidistant from a fixed

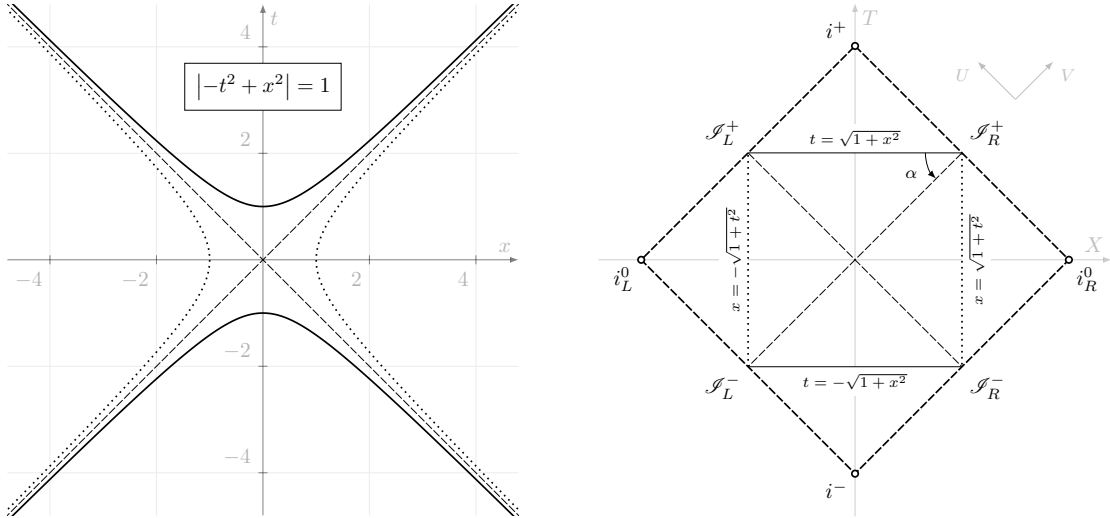


Figure 2: The unit hyperbola  $|-t^2 + x^2| = 1$  consists of four curves. The solid curves inside the null cone,  $|t| > |x|$ , are spacelike. The dotted curves outside the null cone,  $|x| > |t|$ , are timelike. The unit hyperbola—the analog of the unit circle in Euclidean space—is a square on the Penrose diagram of Minkowski space. The future spacelike hyperbola has the angle  $\alpha = -\pi/4$  to the  $V$ -axis at future null infinity. The diagram demonstrates that hyperbolas do not change their causal structure asymptotically. Their causal properties extend to the asymptotic domain.

point, representing the analog of a circle in Euclidean space. It is invariant under Lorentz transformations, just as a circle is under rotations. It is a negatively curved space with two asymptotes,  $t \pm x = 0$ , which are the null rays emanating from the origin. The equation for the hyperbola with (pseudo-)radius  $\tau$  centered at the origin is

$$|-t^2 + x^2| = \tau^2. \quad (4)$$

The unit hyperbola with  $\tau = 1$  is depicted in Fig. 2 in standard coordinates on the left and Penrose coordinates on the right. Its asymptotes are plotted as dashed lines emanating from the origin. It is neat that the analog of the unit circle in Euclidean space is a square on the Penrose diagram of Minkowski space.

We are primarily interested in spacelike hyperbolas for constructing time functions. The unit hyperbolas centered at the origin are spacelike in the interior of the null cone with  $|t| > |x|$ . Future hyperbolas are in  $t > |x|$ , and past hyperbolas are in  $t < -|x|$  (see the shaded regions in Fig. 5). The following sections will discuss three properties of the future hyperbola relevant for time functions for idealized, asymptotic observers: everywhere spacelike (3.1), a snapshot in time (3.2), and a maximal curve satisfying a variational principle (3.3). These properties suggest that hyperboloidal coordinates are as natural in Lorentzian manifolds as spherical coordinates are in Riemannian manifolds.

### 3.1 Spacelike hyperbolas are spacelike everywhere

The future hyperbola on the left panel of Fig. 2 seems to become “asymptotically null.” The curve clearly asymptotes to the null cone and, therefore, to null infinity. In that sense, one could call it asymptotically null [36, 37]. However, the hyperbola does not become causally null. The perception that the hyperbola becomes causally null in the asymptotic domain arises from its representation in standard coordinates. The global causal nature of the hyperbola cannot be discussed faithfully in standard coordinates as they are unsuitable in the asymptotic domain. It is evident from the Penrose diagram on the right panel of Fig. 2 that the future hyperbola is spacelike everywhere, including the asymptotic domain, because the curve representing the hyperbola crosses null infinity horizontally. In contrast, an asymptotically null curve has a null tangent space and is diagonal at null infinity.

We can explicitly calculate the angle at which the hyperbola transverses null infinity [38, 31]. The calculation is easiest in compactified null coordinates  $\{U, V\}$ . Spacelike hyperbola of radius  $\tau$  satisfy

$$\tau^2 = t^2 - x^2 = uv = \tan U \tan V.$$

We calculate the angle of incidence  $\alpha$  that the future hyperbola makes with the  $V$ -axis at the right future null infinity,  $\mathcal{I}_R^+ = \{V = \pi/2\}$  (see Fig. 2). An asymptotically null curve would have an angle of 0 or  $-\pi/2$ . The graph  $U(V)$  for constant values of  $\tau^2$  has an angle of incidence given by

$$\tan \alpha|_{\mathcal{I}_R^+} = \left. \frac{dU}{dV} \right|_{V=\frac{\pi}{2}} = \left. \frac{d}{dV} \left( \arctan \frac{\tau^2}{\tan V} \right) \right|_{V=\frac{\pi}{2}} = -\tau^2.$$

For any non-vanishing, finite  $\tau$ , this angle is in the range  $(-\pi/2, 0)$ . For the unit hyperbola with  $\tau = 1$ , we have  $\alpha = -\pi/4$ , giving the horizontal line in the Penrose diagram Fig. 2. At the limiting values of  $\tau$  we get asymptotically null curves: for  $\tau = 0$  the curve becomes tangent to the  $V$ -axis with  $\alpha = 0$ ; for  $\tau \rightarrow \infty$ , the curve becomes tangent to the  $U$ -axis with  $\alpha \rightarrow -\pi/2$ . Curves for different values of  $\tau$  are depicted in Fig. 5, where one can see this behavior. Note that the particular value of the angle is not important for the qualitative discussion and will depend on the choice of coordinates. The important point is that the future hyperbola is spacelike everywhere, including in the asymptotic domain.

Asymptotically null curves in the Penrose compactification have a vanishing derivative in  $V$  at future null infinity, implying that the linear term in the Taylor series of the graph  $U(V)$  around  $V = \pi/2$  vanishes. We translate this local condition in compactified coordinates to an asymptotic condition in standard coordinates to give a condition for an embedded curve,  $t(x)$ , that behaves like the future hyperbola. For such a curve to be spacelike at null infinity, we require that the  $1/x$ -term does not vanish in the expansion of the embedding,

$$t(x) = x + \frac{C}{x} + \mathcal{O}(x^{-2}), \quad C \neq 0, \quad \text{as } x \rightarrow \pm\infty. \quad (5)$$

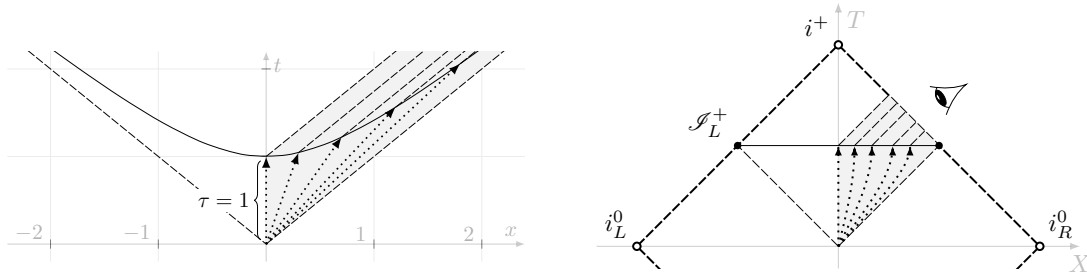


Figure 3: Timekeepers synchronize their clocks at the origin and travel towards an observer at different relative speeds. They send light signals to the idealized observer at infinity at unit proper time. The spacelike curve that connects the timekeepers is the unit hyperbola, which provides a natural snapshot for idealized observers at infinity.

The constant term is absorbed in the definition of the time function. As an example, below is the large  $x$  expansion for the unit hyperbola

$$t(x) = \sqrt{1 + x^2} = x + \frac{1}{2x} + \mathcal{O}(x^{-3}).$$

The term asymptotically null depends on the compactification. We discuss examples of asymptotically null curves in Sec. 5.2 and explore their dependence on compactification in Sec. 5.3.

One can understand that the hyperbola does not become asymptotically null by considering hyperbolic geometry. The hyperbola, or its higher-dimensional version, the hyperboloid, represents a model for hyperbolic geometry—a *homogeneous* space of constant negative curvature [1, 2, 39]. The induced metric on the hyperboloid is the Riemannian metric of hyperbolic space, indicating that the hyperboloid is a spacelike surface everywhere, including the ideal points at infinity. This property of the hyperboloid allows us to employ it as a snapshot in time.

### 3.2 The future hyperbola is a natural snapshot in time

We have seen that hyperbolas inside the null cone are spacelike curves everywhere. Any spacelike curve can serve as a snapshot, but generally, the associated observers are not naturally related to each other. The hyperbola has a particular property that provides a natural notion of a snapshot in Minkowski space.

Consider a family of observers with synchronized clocks at the origin, called timekeepers. The timekeepers move toward an idealized observer to the right at different speeds. These speeds can be stochastically distributed. Each timekeeper sends a light signal to the idealized observer at infinity at their proper time  $\tau$ . The curve that connects the timekeepers at equal proper time and serves as a snapshot for the observer is the future hyperbola  $\tau = \sqrt{t^2 - x^2}$  (see Fig. 3). We can pick any other point  $\{t_0, x_0\}$  to synchronize the timekeepers and perform a similar construction with  $\tau = \sqrt{(t - t_0)^2 - (x - x_0)^2}$ .



This notion of a snapshot works well with asymptotic observers of radiation. Any time function constructed by an observer at infinity is related to a hyperbolic time function by a smooth transformation. In contrast, the transformation from the standard time coordinate to hyperbolic or null coordinates is singular at infinity. Therefore, a time function for observers at infinity must resemble a hyperbola in its asymptotic behavior.

This construction is only valid for the observer side of the hyperboloid. Signals from left-moving timekeepers reach the idealized observer on the right much later because hyperbolas are not time-reversal symmetric. They are adapted to null rays propagating to a null horizon—more on this when we discuss energy decay in Sec. 4.3.

### 3.3 The hyperbola is a maximal curve

The circle is the simplest nontrivial example of a minimal curve solving the isoperimetric problem in the plane: enclosing the largest area with a fixed perimeter [40]. Since the hyperbola is the relativistic analog of a circle, we may expect that the hyperbola solves a similar type of isoperimetric problem.

We can think of the isoperimetric problem as a constrained variational problem. An equivalent problem to maximizing the area with a fixed perimeter is minimizing the perimeter with a fixed area. The action for a minimal curve with length  $L$  enclosing a fixed area  $A$  is

$$S = L - \lambda \cdot A. \quad (6)$$

The solution of this minimization problem is a circle of radius  $1/\lambda$ . The inverse radius, or equivalently, the Lagrange multiplier of the minimization problem  $\lambda$ , is the constant curvature of the circle.

In Minkowski space, minimizing length is not an interesting problem because null rays have zero length. Instead, in Lorentzian variational problems, we look for a maximizing curve. The action for maximizing boundary length is the same as (6), except that the length  $L$  and the area  $A$  are computed for the Minkowski metric (1). This idea generalizes to higher dimensions and curved spacetimes, leading to the analysis of constant mean curvature surfaces in general relativity [41, 42, 43, 44].

Consider a curve parametrized by  $x$  as  $t = t(x)$ . The length of the curve is

$$L = \int ds = \int \sqrt{-dt^2 + dx^2} = \int_{-\infty}^{\infty} \sqrt{-t'(x)^2 + 1} dx,$$

where  $t'(x) = dt(x)/dx$ . We need a reference curve to calculate the enclosed spacetime area. Since we are performing the calculation in standard coordinates, we take the  $t = 0$  line as a reference (see Fig. 4), but the outcome is independent of the reference curve. The enclosed spacetime area by the curve  $t(x)$  and the line  $t = 0$  is

$$A = \int_{-\infty}^{\infty} dx \int_0^{t(x)} dt = \int_{-\infty}^{\infty} t(x) dx. \quad (7)$$

We can write the action (6) as an integral over a Lagrangian density functional

$$S = \int_{-\infty}^{\infty} \mathcal{L} dx = \int_{-\infty}^{\infty} \left[ \sqrt{1 - t(x)^2} - \lambda t(x) \right] dx.$$

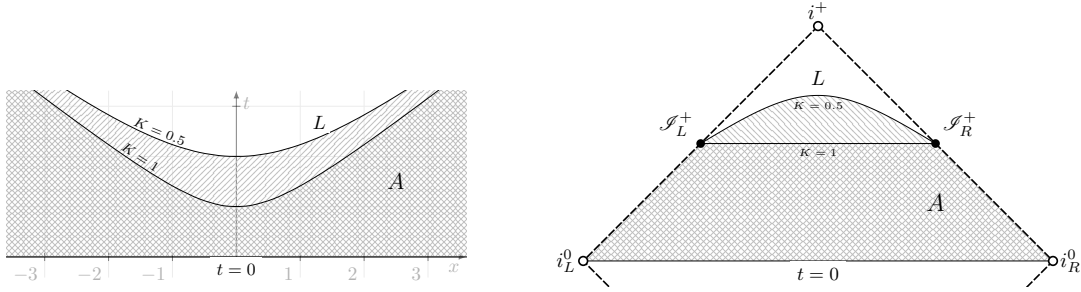


Figure 4: The isoperimetric problem in two-dimensional Minkowski space is to maximize the length  $L$  of a curve  $t(x)$  that encloses a given spacetime area  $A$  with respect to a reference surface, arbitrarily taken as the  $t = 0$  slice. Hyperbolas are solutions to this isoperimetric problem and have constant mean curvature. The upper hyperbola with a smaller mean curvature  $K = 0.5$  encloses a larger spacetime area than the lower hyperbola with a larger mean curvature  $K = 1$ .

The Euler-Lagrange equation for varying  $t(x)$  with respect to the parameter  $x$  reads

$$\frac{d}{dx} \frac{\partial \mathcal{L}}{\partial t'} = \frac{\partial \mathcal{L}}{\partial t} \quad \Rightarrow \quad \frac{d}{dx} \frac{t'}{\sqrt{1-t'^2}} = \lambda.$$

We integrate by  $x$  and solve for  $t'$  with the boundary condition  $t'(0) = 0$

$$t'(x) = \pm \frac{\lambda x}{\sqrt{1 + \lambda^2 x^2}}.$$

Choosing the positive sign and integrating again, we obtain the future hyperbola

$$t(x) = \sqrt{\frac{1}{\lambda^2} + x^2}. \quad (8)$$

The Lagrangian multiplier  $\lambda$  is inversely related to the radius of the hyperbola  $\tau$  and represents the constant mean extrinsic curvature of the curve,  $K = \lambda$ , just as in the Euclidean case. The variational problem (6) does not determine the Lagrangian multiplier,  $\lambda$ , or equivalently, the mean curvature  $K$ . Its value depends inversely on the spacetime area  $A$  we prescribe in the constraint<sup>1</sup>. The larger the spacetime area to be enclosed, the smaller the mean curvature of the hyperbola. In Fig. 4, the upper line with  $K = 0.5$  encloses a larger area than the lower line with  $K = 1$ . The maximal area is enclosed by a curve with vanishing mean curvature,  $K = 0$ . Such maximal slices are level sets of  $t$ .

## 4 Hyperbolic time functions

The future hyperbola is spacelike everywhere and has a natural interpretation as a snapshot in time constructed by an idealized observer at infinity. We want to describe

<sup>1</sup>We can compute the dependence of spacetime area  $A$  on mean curvature  $K$  by evaluating the integral (7) using the curve (8) and taking out the leading term. The result is  $\mathcal{O}(\log K/K^2)$

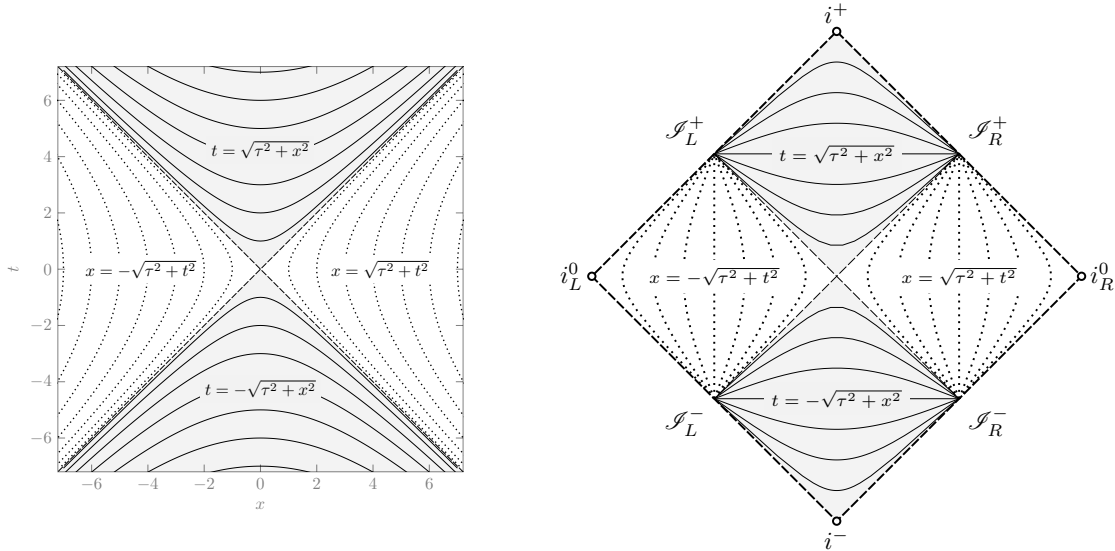


Figure 5: Slicing of Minkowski space by hyperbola of different radii (Milne slicing). The slices asymptote to the same null cone, intersecting at null infinity and becoming singular. The slicing does not respect the time-translation symmetry of Minkowski space, and the metric depends on Milne time (9).

dynamical evolution by parametrizing spacetime using a foliation of such snapshots as given by level sets of a time function. The time function should be suitable for describing the global causal structure in an operationally meaningful way. We have seen that the standard time coordinate is unsuitable for this purpose. We will now construct time functions based on hyperbolas.

## 4.1 Milne time

The first attempt to construct a suitable time function based on hyperbolas is to parametrize Minkowski space by hyperbolas of different radii, as in the case of Euclidean space with polar coordinates based on circles of different radii. This approach goes back to Milne [45], who considered the resulting metric a cosmological model [46]. Many early works on hyperboloidal methods used a similar approach [47, 48, 49, 50, 51, 52]. In higher dimensions, Milne slicing leads to a metric whose time slices have the same geometry as Anti-de Sitter time slices. Therefore, this approach is appealing in recent works on quantum field theory and flat-space holography [53, 54, 55, 56, 57, 58, 59].

The hyperbola of radius  $\tau$  is given by the equation (4). The corresponding parametrization of Minkowski space is depicted in Fig. 5. The figure shows that Milne slices have different causal properties in different parts of the light cone centered at the origin. Outside the light cone, Milne slices are timelike curves representing uniformly accelerated observers. These domains are known as Rindler wedges [60]. The light cone acts as a null horizon for the Rindler wedges.

Inside the light cone, Milne slices are spacelike curves and provide a time function.

We are particularly interested in parametrizing the future light cone by hyperbolas with Milne time  $\tau = \sqrt{t^2 - x^2}$ . Parametrizing the future light cone by the proper time of observers with arbitrary velocity seems a natural choice (compare Sec. 3.2). Each slice has a constant mean extrinsic curvature, but the value of the curvature depends on time as  $K = 1/\tau$ .

To write the Minkowski metric in Milne slicing in its simplest form, we define the comoving coordinate  $\chi$  via  $t = \tau \cosh \chi$  and  $x = \tau \sinh \chi$ . The metric becomes

$$ds^2 = -d\tau^2 + \tau^2 d\chi^2. \quad (9)$$

Milne slicing has some undesirable properties for describing time evolution. First, we see from Fig. 5 that the slices intersect at null infinity and do not provide a smooth foliation of the conformal boundary. This behavior of Milne slices near null infinity is similar to standard time slices near spatial infinity. We can see this by writing the evolution vector field  $\partial_\tau$  in compactified null coordinates

$$\partial_\tau = \frac{1}{\sqrt{\tan U \tan V}} [\sin(2U)\partial_U + \sin(2V)\partial_V].$$

The evolution vector field vanishes at null infinity where  $|U| = \pi/2$  or  $|V| = \pi/2$ . The point at which the slices intersect null infinity is a fixpoint of the slicing. Another way to see the fixpoint is to map the unbounded space dimension to a bounded domain,  $\sin \chi = \tan \rho$ . The metric becomes

$$ds^2 = \frac{1}{\cos^2 \rho} (-\cos^2 \rho d\tau^2 + \tau^2 d\chi^2),$$

The inverse of the conformal metric is singular at  $\rho = \pi/2$ . The boundary is a fixpoint of the time flow<sup>2</sup>.

The second problem is that Milne slicing does not preserve the timelike Killing field  $\partial_t$ , leading to a time-dependent metric (9). While the choice of coordinates is a matter of taste and depends on the problem, introducing an artificial time dependence into the metric is undesirable for many applications.

A related problem is that the light cone at the origin plays a unique role in Milne slicing because it only parametrizes inside the future light cone. This is similar to the role that the origin plays in polar coordinates, around which rotational symmetry is defined. However, it is unclear why the origin should play such a unique role when we describe time evolution in Minkowski space. Note that polar coordinates parametrize all of space, whereas the Milne time is restricted to inside the light cone. In the next section, we will resolve these issues by constructing a hyperbolic foliation that respects the time translation symmetry of Minkowski space and is regular at null infinity.

---

<sup>2</sup>For those familiar with the ADM decomposition [61], another way to see this is to calculate the lapse function describing the passage of time,  $N = \cos \rho$ . Milne time freezes at the boundary.

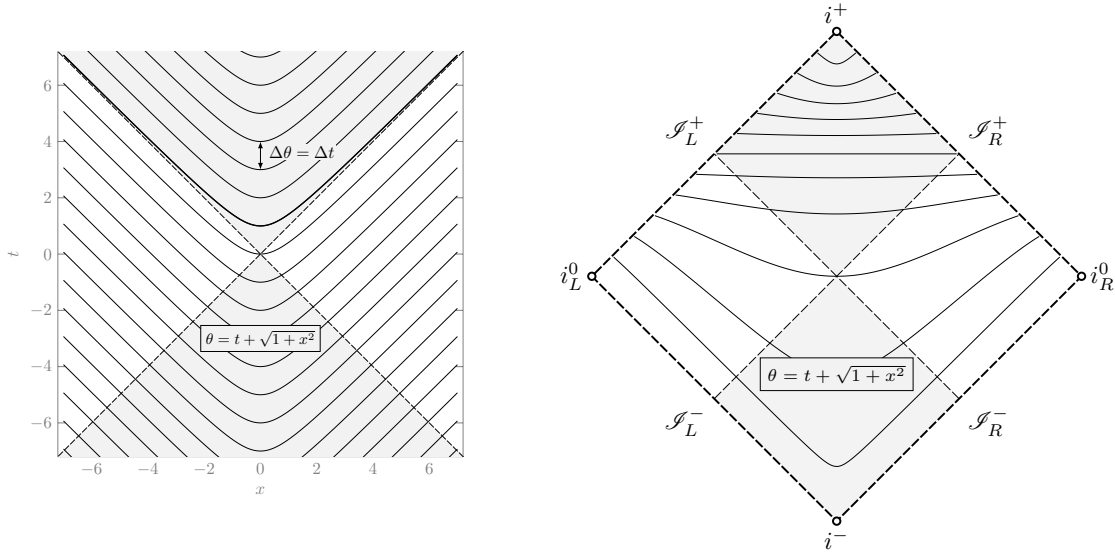


Figure 6: Hyperbolic foliation (10) fixes a future hyperbola and drags it along the timelike Killing field. The resulting metric (12) is independent of time. The null cone through the origin is shaded in gray to contrast with the Milne slicing of Fig. 5.

## 4.2 Hyperbolic foliation

The Milne model (9) uses the radii of hyperbolas as the time coordinate, similar to how polar coordinates use the radii of circles as a space coordinate. However, Euclidean space has no null cone or a time direction. The time-translation symmetry in Minkowski space plays a central role in many applications, and we should keep it in our coordinates.

Instead of slicing the spacetime by hyperbolas of different radii, we fix the radius of a hyperbola to some value,  $L$ , and drag it along the timelike Killing field by  $\theta$  [62, 63, 64, 65].

$$(t - \theta)^2 - x^2 = L^2. \quad (10)$$

We call the slicing of Minkowski space with the time function  $\theta$  a hyperbolic foliation. Solving the above equation for  $\theta$ , we can choose the sign for future or past hyperbolic foliations that foliate future or past null infinity. The future hyperbolic foliation is depicted in Fig. 6. Each slice asymptotes to a future null cone shifted in time. We write the time function  $\theta$  as

$$\theta = t - \sqrt{L^2 + x^2} = t - \frac{L}{\cos \rho}, \quad (11)$$

where  $x = L \tan \rho$  is a scaled spatial compactification.

This time function has many appealing properties. It preserves the timelike Killing field,  $\partial_t = \partial_\theta$ . The mean extrinsic curvature is constant in space and time,  $K = 1/L$ .

The metric is time-independent by construction

$$ds^2 = -d\theta^2 - \frac{2x}{\sqrt{L^2 + x^2}} d\theta dx + \frac{L^2}{L^2 + x^2} dx^2 = \frac{1}{\cos^2 \rho} (-\cos^2 \rho d\theta^2 - 2L \sin \rho d\theta d\rho + L^2 d\rho^2). \quad (12)$$

We can absorb the radius of the hyperbola,  $L$ , in the conformal factor using a rescaled time coordinate  $\bar{\theta} = L\theta$ . As we have seen in Sec. 3.2, the radius of the hyperbola corresponds to the proper time from the origin, so the conformal metric with the rescaled time is scale-free. The conformal metric is regular at null infinity and includes a non-diagonal term indicating that space flows outward in the future hyperbolic foliation. This outflow behavior is analogous to the inflow behavior in the river model of black holes where regular foliations respecting the timelike Killing field have a diagonal shift term [13, 14].

### 4.3 Energy conservation and decay

Noether's theorem states that the symmetries of the background imply conserved quantities for the dynamics. In Minkowski space, we have a time-translation symmetry implying conservation of energy. It is a standard result that energy is conserved for non-dissipative systems. As a simple demonstration, consider the homogeneous wave equation for a scalar field  $\phi(t, x)$

$$-\phi_{tt} + \phi_{xx} = 0,$$

where the subscript is shorthand for a partial derivative. This equation was first written by d'Alembert in 1747 to describe the problem of a vibrating string, long before the unification of space and time into spacetime [66]. Remarkably, the scalar wave equation, with its finite propagation speed, is inherently relativistic in natural units. We write the equation as a conservation law to demonstrate energy conservation

$$\mathcal{E}_t = \mathcal{F}_x, \quad \text{with} \quad \mathcal{E} = \frac{1}{2} (\phi_t^2 + \phi_x^2), \quad \mathcal{F} = \phi_t \phi_x.$$

This form of the wave equation gives us the energy density  $\mathcal{E}$  and the flux density  $\mathcal{F}$ .<sup>3</sup> The total energy is the integral of the energy density over space,  $E = \int_{-\infty}^{\infty} \mathcal{E} dx$ . The scalar field in the standard time coordinate has globally conserved energy, assuming that the boundary terms vanish due to the finite speed of propagation,

$$\frac{dE}{dt} = \int_{-\infty}^{\infty} \frac{d\mathcal{E}}{dt} dx = \int_{-\infty}^{\infty} \frac{d\mathcal{F}}{dx} dx = \phi_t \phi_x \Big|_{-\infty}^{\infty} = 0.$$

However, our experience with isolated dynamical systems suggests they lose energy to radiation. We want a formula that relates the energy decay to radiation flux at null infinity. In null coordinates, the energy calculated along null infinity (also called

---

<sup>3</sup>We can also compute these quantities from the energy-momentum tensor of a scalar field contracted with the timelike Killing vector, but the formulation as a conservation law seems simpler requiring only the formation of total derivatives in the wave equation [67].

Bondi energy after [68]) readily captures such decay. We have seen that the standard time coordinate does not capture the asymptotic behavior adequately. One might anticipate, therefore, that slices approaching null infinity instead of spatial infinity will capture the energy loss. To see if that is the case, we compute the wave equation in Milne coordinates

$$-\phi_{\tau\tau} + \frac{1}{\tau^2}\phi_{\chi\chi} - \frac{1}{\tau}\phi_{\tau} = 0.$$

We compactify space with  $\sin \chi = \tan \rho$  to analyze the asymptotic behavior,

$$-\frac{\tau^2}{\cos \rho}\phi_{\tau\tau} + \cos \rho \phi_{\rho\rho} - \frac{\tau}{\cos \rho}\phi_{\tau} - \sin \rho \phi_{\rho} = 0.$$

The energy and flux densities are

$$\mathcal{E} = \frac{1}{2} \left( \frac{\tau^2}{\cos \rho}\phi_{\tau}^2 + \cos \rho \phi_{\rho}^2 \right), \quad \mathcal{F} = \cos \rho \phi_{\tau}\phi_{\rho}.$$

Energy is conserved also in Milne time,

$$\frac{dE}{d\tau} = \int_{-\frac{\pi}{2}}^{\frac{\pi}{2}} \frac{d\mathcal{F}}{d\rho} d\rho = \cos \rho \phi_{\tau}\phi_{\rho} \Big|_{-\frac{\pi}{2}}^{\frac{\pi}{2}} = 0.$$

Energy conservation is not just a consequence of evaluating the energy at spatial infinity. It is a consequence of the intersection of time slices in the asymptotic domain. To model energy radiation to infinity, we need an asymptotically regular foliation. Switching to a hyperbolic foliation makes the loss of energy explicit. The transformed wave equation in hyperbolic foliation  $\theta$  and compactifying coordinate  $\rho$  reads after a division by  $\cos^2 \rho$

$$-\phi_{\theta\theta} - 2 \sin \rho \phi_{\theta\rho} + \cos^2 \rho \phi_{\rho\rho} - \cos \rho \phi_{\theta} - 2 \sin \rho \cos \rho \phi_{\rho}\phi = 0.$$

The energy and flux densities are

$$\mathcal{E} = \frac{1}{2} (\phi_{\theta}^2 + \cos^2 \rho \phi_{\rho}^2), \quad \mathcal{F} = -\sin \rho \phi_{\theta}^2 + \cos^2 \rho \phi_{\theta}\phi_{\rho}.$$

Now we can show that a Bondi-type total energy is not conserved but decays due to radiation across null infinity,

$$\frac{d}{d\theta} E = \int_{-\frac{\pi}{2}}^{\frac{\pi}{2}} \frac{d\mathcal{F}}{d\rho} d\rho = \mathcal{F} \Big|_{-\frac{\pi}{2}}^{\frac{\pi}{2}} = -\phi_{\theta}^2 \Big|_{\mathcal{I}_R^+} - \phi_{\theta}^2 \Big|_{\mathcal{I}_L^+} \leq 0.$$

One can understand the behavior of energy by visually inspecting the Penrose diagrams in Figs. 1, 5, and 6. An outgoing characteristic in standard time and Milne time crosses all slices because each level set of the corresponding time function ends at the same asymptotic point. In hyperbolic foliation, however, an outgoing null ray carrying energy will intersect only a finite number of slices. Therefore, energy will decay along a hyperbolic foliation. The propagation of such energy packages along null rays is best visualized by the characteristics of the metric plotted in Fig. 7. Outgoing characteristics leave the domain through the conformal boundary only in the case of the hyperbolic foliation (right-most panel).

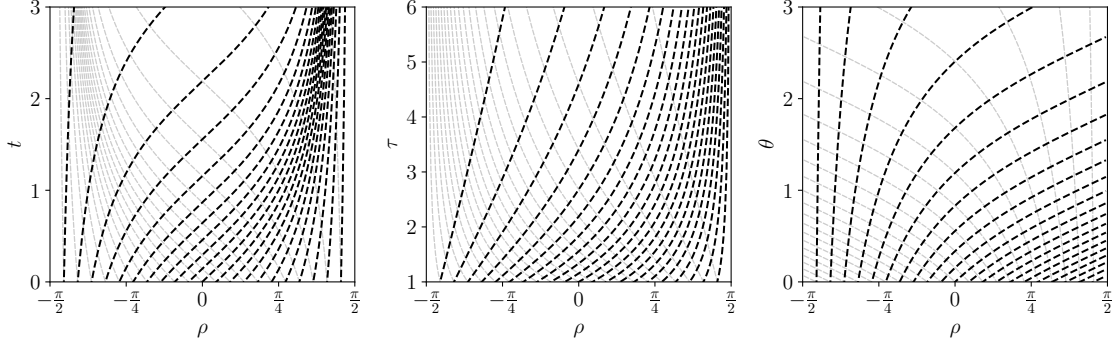


Figure 7: Null rays in the compactified space coordinate  $\rho \in (-\pi/2, \pi/2)$  for the standard time  $t$  on the left, Milne time  $\tau$  in the middle, and hyperbolic foliation  $\theta$  on the right. Outgoing null rays in standard time and Milne time never reach the conformal boundary. Compare to the Penrose diagrams in Figs. 1, 5, and 6.

## 5 Hyperboloidal surfaces

The hyperbolic foliation has desirable properties for parameterizing the asymptotic domain. In this section, we present generalizations based on these properties. The objective is to demonstrate that hyperboloidal time functions are generic and adaptable to various scenarios.

### 5.1 Higher dimensions

The hyperbolic foliation (11) is based on hyperbola in one space dimension. In higher dimensions, we use the radial coordinate  $r \in [0, \infty)$  instead of  $x \in (-\infty, \infty)$ , and the hyperbola becomes the two-sheeted hyperboloid of revolution.

Our discussion from previous sections generalizes to higher dimensions with minor modifications. The  $n$ -dimensional Minkowski metric in spherical coordinates reads

$$ds^2 = -dt^2 + dr^2 + r^2 d\sigma_{n-2}^2,$$

where  $d\sigma_{n-2}^2$  is the metric on the unit  $(n-2)$ -sphere and  $r$  is the areal coordinate. The areal coordinate has the domain  $r \in [0, \infty)$ , so the Penrose diagrams are not squares but triangles. The level sets of the time function  $\theta = t - \sqrt{L^2 + r^2}$  are hyperboloids of revolution. The analogous metric to (12) is obtained by replacing  $x$  with  $r$ ,

$$ds^2 = -d\theta^2 - \frac{2r}{\sqrt{L^2 + r^2}} d\theta dr + \frac{L^2}{L^2 + r^2} dr^2 + r^2 d\sigma_{n-2}^2.$$

The induced metric on the level sets of  $\theta$  is the homogeneous metric of hyperbolic geometry with constant, negative curvature. The slices have the same geometry as slices of Anti-de Sitter space in standard coordinates. This foliation combined with compactification is useful for numerical calculations investigating wave equations in Minkowski space [65, 69].



## 5.2 Hyperboloidal time functions

The essential property of the time-shifted hyperboloids (10) is that they allow us to describe dynamical evolution starting with initial data on an instant of time for the idealized observer at infinity, where we can measure the energy carried out by outgoing radiation. We require that the time function is spacelike everywhere and that the level sets provide a foliation of null infinity. These two properties define *hyperboloidal* foliations [12]. Among hyperboloidal foliations, choosing those that preserve the timelike-translation symmetry of the background is often desirable. Subsequent compactification of space brings the conformal boundary to a fixed coordinate location independent of time. Such hyperboloidal foliations are called *scri-fixing* [70] (or scri-freezing for conformal Einstein equations [71]) because they fix the conformal boundary, scri, to a time-independent coordinate location. In Minkowski space and general stationary spacetimes, scri-fixing hyperboloidal foliations can be constructed using the height function technique [70]. The relationship between the standard time  $t$  and hyperboloidal time  $\theta$  is, up to trivial scalings,

$$\theta = t + h(r), \quad (13)$$

where  $h$  is referred to as the height function because it describes the “height” of the spacelike surface with respect to  $t$  at each  $r$  [72]. The height function preserves the spherical and time-translation symmetries of the background because it is independent of the angular and time coordinates. The Minkowski metric reads

$$ds^2 = -d\theta^2 + 2H(r) d\theta dr + (1 - H(r)^2) dr^2 + r^2 d\sigma_{n-2}^2, \quad (14)$$

where  $H(r) := dh/dr$  is called the boost function. For  $H(r) = \pm 1$ , or equivalently  $h(r) = \pm r$ , we get null coordinates. Scri-fixing hyperboloidal foliations satisfy

$$|H(r)| < 1 \quad \forall r \in [0, \infty) \quad \& \quad |H(r)| = 1 - \frac{C}{r^2} + \mathcal{O}(r^{-3}), \text{ as } r \rightarrow \infty, \quad (15)$$

with some constant  $C > 0$ . The first condition ensures the  $\theta$ -hypersurfaces are space-like, providing a time function. The second condition ensures the  $\theta$ -hypersurfaces are hyperboloidal (compare (5)). The sign of  $H$  determines whether the foliation is future-directed or past-directed, meaning whether  $\theta$  asymptotes to outgoing null rays  $u$  or incoming null rays  $v$ . The constant  $C$  determines how rapidly our foliation approaches null infinity. For small  $C$ , the foliation resembles a null foliation and has fast characteristics. For large  $C$ , the foliation resembles the standard time coordinate and has slow characteristics.

The off-diagonal term in (14) complicates the expressions but is necessary to keep the time-translation symmetry of the background. The freedom in the spatial transformation can be used to remove the non-diagonal term using a generalization of Lemaître’s construction [73, 74]. For the time transformation (13) with the differential  $d\theta = dt + Hdr$ , we define a space coordinate  $\xi$  via  $d\xi = dt + \frac{1}{H}dr$ . The transformed metric is diagonal but depends on time through  $r = r(\theta, \xi)$ ,

$$ds^2 = \frac{1}{1 - H^2} (-d\theta^2 + H^2 d\xi^2) + r^2 d\sigma_{n-2}^2.$$

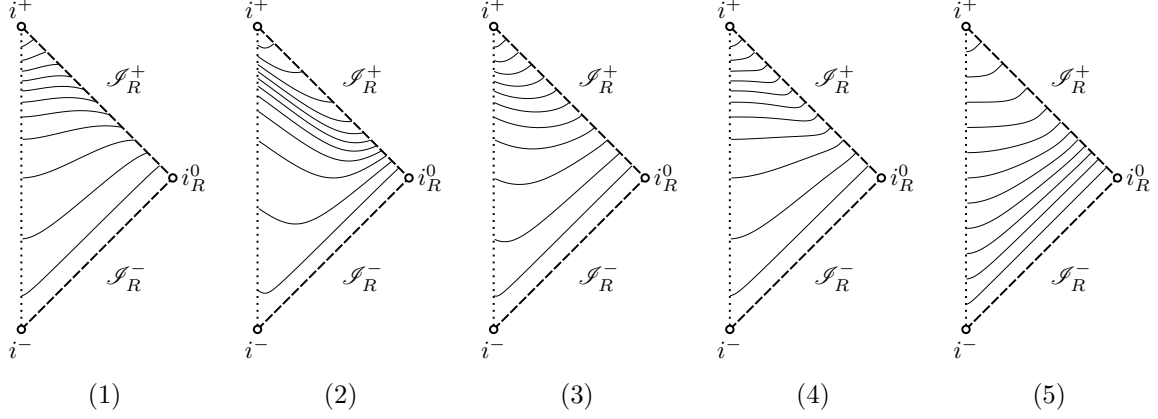


Figure 8: Five examples of foliations corresponding to the five height functions (16) with  $C = 1$ , (17) with  $L = 1$  and  $r_0 = 1$ , (18), (19), and (20). The first two are hyperboloidal; the other three are asymptotically null in the Penrose compactification.

Below are two examples of hyperboloidal height functions.

$$h_1(r) = r + \frac{C}{1+r}, \quad H_1(r) = 1 - \frac{C}{(1+r)^2}, \quad (16)$$

$$h_2(r) = \sqrt{L^2 + (r - r_0)^2}, \quad H_2(r) = \frac{r - r_0}{\sqrt{L^2 + (r - r_0)^2}}. \quad (17)$$

The first example is the simplest height function that satisfies the conditions (15) and is regular at the origin. The second example is an off-centered hyperboloid. It is helpful in scenarios where radiation is emitted from a source near  $r = r_0$  and is absorbed in both directions of the radial coordinate, such as in a black hole spacetime with a particle perturbation.

In contrast, below are asymptotically null height functions.

$$h_3(r) = \sqrt{\frac{1}{1+r} + r^2}, \quad H_3(r) = \frac{2r - \frac{1}{(1+r)^2}}{2\sqrt{\frac{1}{1+r} + r^2}}, \quad (18)$$

$$h_4(r) = r + e^{-r}, \quad H_4(r) = 1 - e^{-r}, \quad (19)$$

$$h_5(r) = \log(\cosh r), \quad H_5(r) = \tanh r. \quad (20)$$

The examples are plotted in Fig. 8. The last three figures cross future null infinity at 45 degrees to the horizontal, indicating that they become asymptotically null. Such height functions are useful near event or cosmological horizons with exponential mappings. We will discuss this in the next section.

The specific choice of the height function is more of an art than a science. Some options are elegant and simplify calculations. Other options provide flexibility in handling different domains of interest but are messy (for an overview in black-hole spacetimes, see [75]). The particular choice depends on the problem at hand, the background, and the compactification one prefers, which we discuss next.

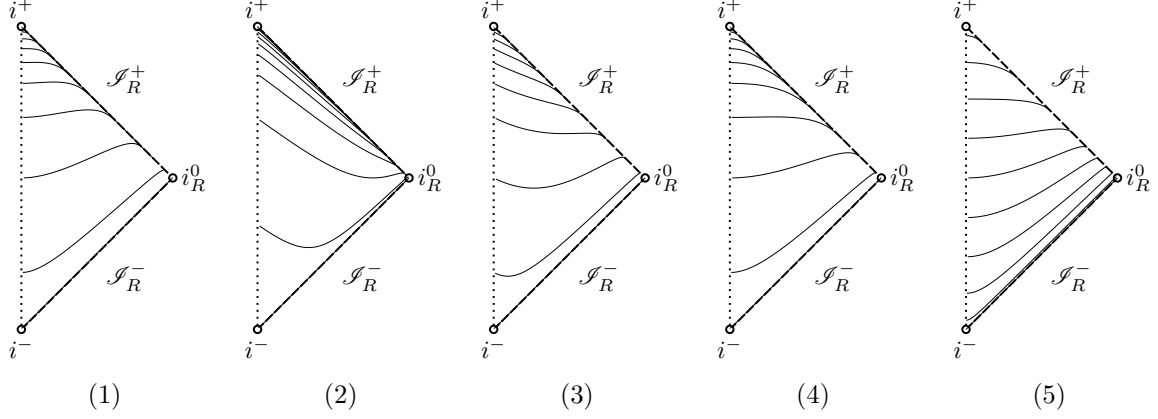


Figure 9: The same foliations as in Fig. 8 but with compactification using the hyperbolic tangent function,  $U = \tanh u$ , and  $V = \tanh v$ . The asymptotically null foliations (3),(4), and (5) become hyperboloidal (spacelike across null infinity) when spacetime is compactified using the exponential hyperbolic tangent function.

### 5.3 Spatial compactifications

In the previous sections, the mapping from the unbounded domain in  $r$  to the bounded domain in  $\rho$  was chosen as the tangent function because of historical reasons. There are infinitely many functions that one can use for compactification. The impact of mappings from unbounded domains to bounded domains have been studied By Grosch and Orszag in in 1977 [76] who distinguish algebraic and exponential mappings (see also [77, 78]).

A compactification involves a mapping  $\rho = g(r)$  from an unbounded domain  $r \in [0, \infty)$  to the bounded domain  $\rho \in [0, S)$  such that

$$g(0) = 0, \quad g(\infty) = S,$$

$$\frac{dg}{dr} =: G(\rho) \geq 0, \quad G(S) = 0.$$

Below are some examples of mappings and their inverse for  $S = 1$ , or  $S = \pi/2$  for the trigonometric mapping. One can add a scaling parameter to these mappings, which can be used to tune the spacing of points near the boundaries or change the domain size from  $S$  to any other value [78].

- Algebraic:

$$r = \frac{\rho}{1 - \rho}, \quad \rho = \frac{r}{1 + r}, \quad G = (1 - \rho)^2. \quad (21)$$

$$r = \frac{2\rho}{1 - \rho^2}, \quad \rho = \frac{-1 + \sqrt{1 + r^2}}{r}, \quad G = \frac{(1 - \rho^2)^2}{2(1 + \rho^2)}, \quad (22)$$

$$r = \tan \rho, \quad \rho = \arctan r, \quad G = \cos^2 \rho. \quad (23)$$

- Exponential:

$$r = \operatorname{arctanh} \rho = \frac{1}{2} \ln \frac{1 + \rho}{1 - \rho}, \quad \rho = \tanh(r), \quad G(\rho) = (1 - \rho^2). \quad (24)$$

$$r = -\ln(1 - \rho), \quad \rho = 1 - e^{-r}, \quad G = 1 - \rho. \quad (25)$$

Some of the examples above can be used to compress a domain that is unbounded in both directions ((22), (23), and (24)).

For a given compactification, one can define a *characteristic-preserving* hyperboloidal transformation by demanding that the characteristic preserves the coordinate expression of characteristics. For example, we require  $\tau - \rho = t - r$  for outgoing characteristics. This method of constructing suitable hyperboloidal coordinates is useful in numerical calculations [79, 80, 81]. In high-dimensional Minkowski space, only the algebraic mappings can be used with hyperboloidal transformation. The reason is the rate at which spheres grow with radius. To see this, we write the hyperboloidal Minkowski metric (14) in compactifying coordinates,

$$ds^2 = \frac{1}{G} \left( -G d\theta^2 + 2H d\theta d\rho + \frac{1 - H^2}{G} d\rho^2 + Gr^2 d\sigma_{n-2}^2 \right). \quad (26)$$

The regularity of the conformal metric  $d\bar{s}^2 = Gds^2$  at the conformal boundary requires that the metric coefficients  $(1 - H^2)/G$  and  $Gr^2$  are finite. The term  $Gr^2$  vanishes at the boundary for exponential mappings but is finite for algebraic mappings.

The time function (11) can be combined with algebraic compactifications such as (22) or (23). The conformal metric is regular at the boundary,

$$ds^2 = \frac{1}{\cos^2 \rho} \left( -\cos^2 \rho d\theta^2 - 2 \sin \rho d\theta d\rho + d\rho^2 + \sin^2 \rho d\sigma_{n-2}^2 \right) \quad (27)$$

$$= \left( \frac{2}{1 - \rho^2} \right)^2 \left( -\left( \frac{1 - \rho^2}{2} \right)^2 d\theta^2 - 2\rho(1 + \rho^2) d\theta d\rho + d\rho^2 + \rho^2 d\sigma_{n-2}^2 \right). \quad (28)$$

The time slices in the second expression are the high-dimensional analogs of the Poincaré disk model for hyperbolic geometry. The off-diagonal shift term represents the outward flow of space, and the time slices of the conformal metric are spatially flat. This structure is similar to the Schwarzschild geometry in Painlevé-Gullstrand coordinates [13, 14] or the de Sitter geometry in regularized static coordinates [82].

This brings us to a subtle point about the global causal behavior of hyperboloidal surfaces. In 1+1-dimensional Minkowski space, whether a surface is asymptotically null depends on the chosen spacetime compactification. Asymptotically null hypersurfaces with algebraic compactification become hyperboloidal with exponential compactification as illustrated in Fig. 9. While this choice is arbitrary in 1+1-dimensional Minkowski space, it is enforced by the asymptotic growth of spheres in higher dimensions. For example, in Schwarzschild spacetime, the standard radial coordinate is an exponential compactification of the tortoise coordinate toward the event horizon similar to (25) and horizon-penetrating coordinates are hyperboloidal. Such exponential compactifications are useful also in cosmological spacetimes. In asymptotically hyperbolic cosmologies, the transformation (20) can be used in combination with the exponential mapping (24) leading to a hyperboloidal foliation [83].

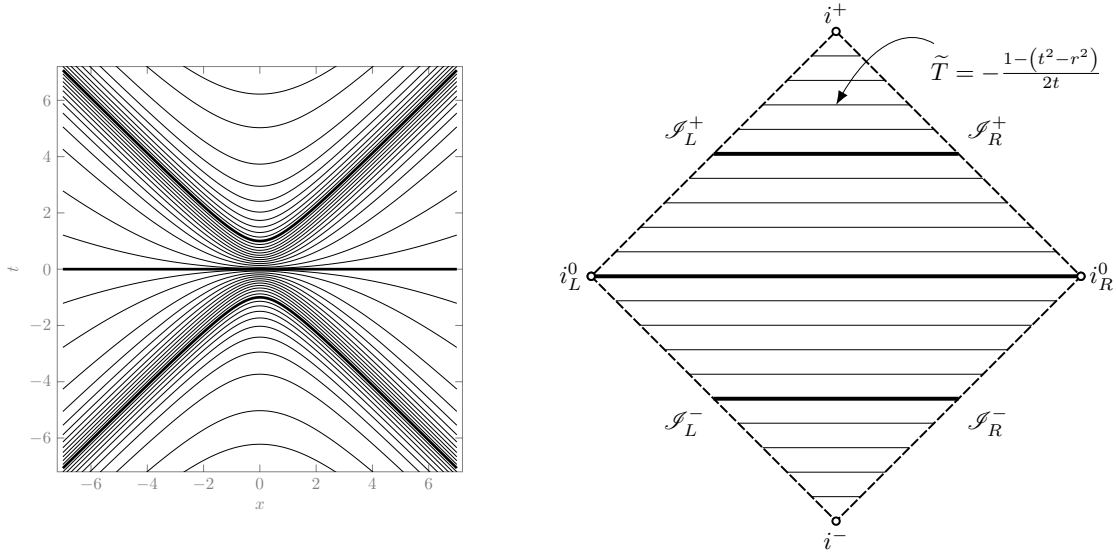


Figure 10: Penrose time slices in standard coordinates on the left and in Penrose coordinates on the right. The three limiting surfaces with  $T = 0$  and  $T = \pm\pi/4$  are drawn as thick lines.

## 5.4 Penrose coordinates are hyperboloidal

We constructed the Penrose coordinates in Sec. 2 by compactifying null coordinates and defining time and space coordinates. We also saw that Penrose coordinates do not arise from the compactification of standard coordinates. It is natural to ask which coordinates lead to Penrose coordinates when compactified. To study this question, we decompactify the time coordinate,

$$\tan(2T) = \tan(V + U) = \tan(\arctan(t + r) + \arctan(t - r)) = \frac{2t}{1 - (t^2 - r^2)}.$$

The Cauchy surface  $t = 0$  maps to  $T = 0$ . The timelike infinities  $t \rightarrow \pm\infty$  map to  $T = \pm\pi/2$ . The null cone from the origin gives the limiting surfaces with  $T = \pm\pi/4$  drawn as thick lines in Fig. 10. The nature of the level sets of  $T \in (0, \pi/2)$  is obvious from the Penrose diagram, but we can get more insight into their geometry by setting  $\tan(2T) \equiv -1/\tilde{T}$ . Then

$$t = \tilde{T} \pm \sqrt{1 + r^2 + \tilde{T}^2}, \quad \text{or} \quad (t - \tilde{T})^2 - r^2 = 1 + \tilde{T}^2.$$

The hyperbolas with time-dependent radii  $\sqrt{1 + \tilde{T}^2}$  are shifted along the standard time  $t$  by  $\tilde{T}$ . This expression combines the Milne slicing consisting of hyperbolas with time-dependent radii (4) and the hyperbolic foliation consisting of hyperbolas shifted along the timelike Killing field (11) (see Fig. 10). We conclude that Penrose coordinates arise from the direct compactification of hyperboloidal coordinates.

## Acknowledgement

I thank members of the Hyperboloidal Research Network for many fruitful interactions. I especially thank Alex Vañó-Viñuales for suggestions on the manuscript. This material is supported by the National Science Foundation under Grant No. 2309084.

## References

- [1] James W Cannon, William J Floyd, Richard Kenyon, Walter R Parry, et al. Hyperbolic geometry. *Flavors of geometry*, 31(59-115):2, 1997.
- [2] Boris A Rosenfeld. *A history of non-Euclidean geometry: Evolution of the concept of a geometric space*, volume 12. Springer Science & Business Media, 2012.
- [3] Scott Walter. The non-Euclidean style of Minkowskian relativity. In Jeremy Gray, editor, *The Symbolic Universe*, pages 91–127. Oxford University PressOxford, July 1999.
- [4] Scott Walter. Breaking in the 4-vectors: the four-dimensional movement in gravitation, 1905–1910. In *The genesis of general relativity*, pages 1118–1178. Springer, 2007.
- [5] Scott Walter. Minkowski’s Modern World. In Vesselin Petkov, editor, *Minkowski Spacetime: A Hundred Years Later*, pages 43–61. Springer Netherlands, Dordrecht, 2010.
- [6] Peter Galison. Minkowski’s space-time: from visual thinking to the absolute world. In *Chrono-topologies*, pages 9–41. Brill, 2010.
- [7] John A. Rhodes and Mark D. Semon. Relativistic velocity space, Wigner rotation, and Thomas precession. *American Journal of Physics*, 72(7):943–960, July 2004.
- [8] Abraham Albert Ungar. *Analytic hyperbolic geometry and Albert Einstein’s special theory of relativity*. World Scientific, 2008.
- [9] Tevian Dray. The geometry of relativity. *American Journal of Physics*, 85(9):683–691, September 2017.
- [10] Tevian Dray. *The geometry of special relativity*. CRC Press, 2021.
- [11] John F Barrett. The hyperbolic theory of special relativity. *arXiv preprint arXiv:1102.0462*, 2011.
- [12] Helmut Friedrich. Cauchy problems for the conformal vacuum field equations in general relativity. *Communications in Mathematical Physics*, 91:445–472, 1983.
- [13] Karl Martel and Eric Poisson. Regular coordinate systems for Schwarzschild and other spherical spacetimes. *American Journal of Physics*, 69(4):476–480, 2001.

- [14] Andrew JS Hamilton and Jason P Lisle. The river model of black holes. *American Journal of Physics*, 76(6):519–532, 2008.
- [15] Rodrigo Panosso Macedo, Benjamin Leather, Niels Warburton, Barry Wardell, and Anil Zenginoğlu. Hyperboloidal method for frequency-domain self-force calculations. *Physical Review D*, 105(10):104033, 2022.
- [16] José Luis Jaramillo. Pseudospectrum and binary black hole merger transients. *Classical and Quantum Gravity*, 39(21):217002, 2022.
- [17] Justin L Ripley. Computing the quasinormal modes and eigenfunctions for the Teukolsky equation using horizon penetrating, hyperboloidally compactified coordinates. *Classical and Quantum Gravity*, 39(14):145009, 2022.
- [18] Christian Peterson, Shalabh Gautam, Inês Rainho, Alex Vañó-Viñuales, and David Hilditch. 3D evolution of a semilinear wave model for the Einstein field equations on compactified hyperboloidal slices. *Physical Review D*, 108(2):024067, 2023.
- [19] Lidia J Gomes Da Silva, Rodrigo Panosso Macedo, Jonathan E Thompson, Juan A Valiente Kroon, Leanne Durkan, and Oliver Long. Hyperboloidal discontinuous time-symmetric numerical algorithm with higher order jumps for gravitational self-force computations in the time domain. *arXiv preprint arXiv:2306.13153*, 2023.
- [20] Charalampos Markakis, Sean Bray, and Anil Zenginoğlu. Symmetric integration of the 1+1 Teukolsky equation on hyperboloidal foliations of Kerr spacetimes. *arXiv preprint arXiv:2303.08153*, 2023.
- [21] Alex Vañó-Viñuales. Spherically symmetric black hole spacetimes on hyperboloidal slices. *arXiv preprint arXiv:2304.05384*, 2023.
- [22] Rodrigo Panosso Macedo. Hyperboloidal approach for static spherically symmetric spacetimes: a didactical introduction and applications in black-hole physics. *Philosophical Transactions of the Royal Society A*, 382(2267):20230046, 2024.
- [23] Dejan Gajic and Maxime Van de Moortel. Late-time tails for scale-invariant wave equations with a potential and the near-horizon geometry of null infinity. *arXiv preprint arXiv:2401.13047*, 2024.
- [24] Philippe G LeFloch and Yue Ma. The Euclidean-hyperboloidal foliation method. Application to f(R) modified gravity. *arXiv preprint arXiv:2312.17712*, 2023.
- [25] Roger Penrose. Asymptotic properties of fields and space-times. *Physical Review Letters*, 10(2):66–68, January 1963.
- [26] Roger Penrose. Zero rest-mass fields including gravitation: asymptotic behaviour. *Proceedings of the Royal Society of London. Series A. Mathematical and Physical Sciences*, 284(1397):159–203, February 1965.

- [27] Robert M Wald. *General relativity*. University of Chicago press, 1984.
- [28] Matthias Blau. *Lecture notes on general relativity*. Albert Einstein Center for Fundamental Physics Bern, 2011.
- [29] Sean M Carroll. *Spacetime and geometry*. Cambridge University Press, 2019.
- [30] Alex Vañó-Viñuales. Conformal diagrams for stationary and dynamical strong-field hyperboloidal slices. *arXiv preprint arXiv:2311.04972*, 2023.
- [31] Juan A Valiente Kroon. *Conformal methods in general relativity*. Cambridge University Press, 2017.
- [32] Werner Israel. Dark stars: the evolution of an idea. *Three hundred years of gravitation*, pages 199–276, 1987.
- [33] José M M Senovilla and David Garfinkle. The 1965 Penrose singularity theorem. *Classical and Quantum Gravity*, 32(12):124008, June 2015.
- [34] NK Nielsen. On the origin of the Gullstrand–Painlevé coordinates. *The European Physical Journal H*, 47(1):6, 2022.
- [35] Klaas Landsman. Penrose’s 1965 singularity theorem: From geodesic incompleteness to cosmic censorship. *General Relativity and Gravitation*, 54(10):115, October 2022. arXiv:2205.01680 [gr-qc, physics:math-ph, physics:physics].
- [36] Gioel Calabrese, Carsten Gundlach, and David Hilditch. Asymptotically null slices in numerical relativity: mathematical analysis and spherical wave equation tests. *Classical and Quantum Gravity*, 23(15):4829, 2006.
- [37] Charles W Misner, James R van Meter, and David R Fiske. Excising das all: Evolving maxwell waves beyond scri. *Physical Review D*, 74(6):064003, 2006.
- [38] Anıl Zenginöglü. A conformal approach to numerical calculations of asymptotically flat spacetimes. *arXiv preprint arXiv:0711.0873*, 2007.
- [39] William F Reynolds. Hyperbolic geometry on a hyperboloid. *The American mathematical monthly*, 100(5):442–455, 1993.
- [40] Viktor Blåsjö. The isoperimetric problem. *The American Mathematical Monthly*, 112(6):526–566, 2005.
- [41] Jerrold E Marsden and Frank J Tipler. Maximal hypersurfaces and foliations of constant mean curvature in general relativity. *Physics Reports*, 66(3):109–139, 1980.
- [42] Dieter R. Brill, John M. Cavallo, and James A. Isenberg.  $K$ -surfaces in the Schwarzschild space-time and the construction of lattice cosmologies. *Journal of Mathematical Physics*, 21(12):2789–2796, December 1980.



- [43] Edward Malec and Niall Ó Murchadha. General spherically symmetric constant mean curvature foliations of the Schwarzschild solution. *Physical Review D*, 80(2):024017, 2009.
- [44] Michael Eichmair and Jan Metzger. Unique isoperimetric foliations of asymptotically flat manifolds in all dimensions. *Inventiones mathematicae*, 194:591–630, 2013.
- [45] Edward Arthur Milne. Relativity, gravitation, and world-structure. *Philosophy*, 11(41), 1936.
- [46] Markus Pössel. Teaching cosmology with special relativity: piecewise inertial frames as a model for cosmic expansion. *European Journal of Physics*, 40(2):025602, 2019.
- [47] Paul AM Dirac. Forms of relativistic dynamics. *Reviews of Modern Physics*, 21(3):392, 1949.
- [48] Y. W. Chen and Hans Lewy. Solutions of the n-Dimensional Wave Equation in the Exterior of the Characteristic Cones (I). *Indiana University Mathematics Journal*, 20(1):33–55, 1970. Publisher: Indiana University Mathematics Department.
- [49] Y. W. Chen and H. Lewy. On the Hyperboloidal Means and the Wave Equation. *Indiana University Mathematics Journal*, 21(5):437–447, 1971. Publisher: Indiana University Mathematics Department.
- [50] Robert S Strichartz. Harmonic analysis on hyperboloids. *Journal of Functional Analysis*, 12(4):341–383, April 1973.
- [51] A DiSessa. Quantization on hyperboloids and full space-time field expansion. *Journal of Mathematical Physics*, 15(11):1892–1900, 1974.
- [52] Charles M Sommerfield. Quantization on spacetime hyperboloids. *Annals of Physics*, 84(1):285–302, May 1974.
- [53] Jan de Boer and Sergey N. Solodukhin. A holographic reduction of Minkowski space-time. *Nuclear Physics B*, 665:545–593, August 2003. arXiv:hep-th/0303006.
- [54] Miguel Campiglia and Alok Laddha. Asymptotic symmetries of QED and Weinberg’s soft photon theorem. *Journal of High Energy Physics*, 2015(7):1–16, 2015.
- [55] Clifford Cheung, Anton de la Fuente, and Raman Sundrum. 4D Scattering Amplitudes and Asymptotic Symmetries from 2D CFT. *Journal of High Energy Physics*, 2017(1):112, January 2017. arXiv:1609.00732 [gr-qc, physics:hep-ph, physics:hep-th].

- [56] Andrew Strominger. *Lectures on the infrared structure of gravity and gauge theory*. Princeton University Press, 2018.
- [57] Naoki Ogawa, Tadashi Takayanagi, Takashi Tsuda, and Takahiro Waki. Wedge Holography in Flat Space and Celestial Holography. *Physical Review D*, 107(2):026001, January 2023. arXiv:2207.06735 [gr-qc, physics:hep-th].
- [58] Charlotte Sleight and Massimo Taronna. Celestial holography revisited. *arXiv preprint arXiv:2301.01810*, 2023.
- [59] Hong Zhe Chen, Robert C Myers, and Ana-Maria Raclariu. Entanglement, Soft Modes, and Celestial Holography. *arXiv preprint arXiv:2308.12341*, 2023.
- [60] W Rindler. Hyperbolic motion in curved space time. *Physical Review*, 119(6):2082, 1960.
- [61] Richard Arnowitt, Stanley Deser, and Charles W Misner. Republication of: The dynamics of general relativity. *General Relativity and Gravitation*, 40:1997–2027, 2008.
- [62] Vince Moncrief. Conformally regular ADM evolution equations, 2000. <http://online.itp.ucsb.edu/online/numrel00/moncrief>.
- [63] Lars Andersson. Construction of hyperboloidal initial data. In *The Conformal Structure of Space-Time: Geometry, Analysis, Numerics*, pages 183–194. Springer, 2002.
- [64] Sascha Husa. Numerical relativity with the conformal field equations. In *Current Trends in Relativistic Astrophysics: Theoretical, Numerical, Observational*, pages 159–192. Springer, 2003.
- [65] G. Fodor and I. Racz. What does a strongly excited 't Hooft-Polyakov magnetic monopole do? *Physical Review Letters*, 92:151801, 2004. arXiv:hep-th/0311061.
- [66] Agamenon RE Oliveira. D'Alembert and the Wave Equation: Its Disputes and Controversies. *Advances in Historical Studies*, 9(04):229, 2020.
- [67] Piotr Bizoń, Bradley Cownden, and Maciej Maliborski. Characteristic approach to the soliton resolution. *Nonlinearity*, 35(8):4585, 2022.
- [68] Hermann Bondi, M Gr J Van der Burg, and AWK Metzner. Gravitational waves in general relativity, VII. Waves from axi-symmetric isolated system. *Proceedings of the Royal Society of London. Series A. Mathematical and Physical Sciences*, 269(1336):21–52, 1962.
- [69] Piotr Bizoń and Anil Zenginoğlu. Universality of global dynamics for the cubic wave equation. *Nonlinearity*, 22(10):2473, 2009.
- [70] Anil Zenginoğlu. Hyperboloidal foliations and scri-fixing. *Classical and Quantum Gravity*, 25(14):145002, 2008.

- [71] Jörg Frauendiener. Numerical treatment of the hyperboloidal initial value problem for the vacuum Einstein equations. II. The evolution equations. *Physical Review D*, 58(6):064003, 1998.
- [72] Robert Beig and N Ó Murchadha. Late time behavior of the maximal slicing of the Schwarzschild black hole. *Physical Review D*, 57(8):4728, 1998.
- [73] Georges Lemaître. L'univers en expansion. In *Annales de la Société scientifique de Bruxelles*, volume 53, page 51, 1933.
- [74] Abbé Georges Lemaître. The Expanding Universe. *General Relativity and Gravitation*, 29(5):641–680, May 1997.
- [75] Rodrigo Panosso Macedo. Hyperboloidal framework for the kerr spacetime. *Classical and Quantum Gravity*, 37(6):065019, 2020.
- [76] Chester E Grosch and Steven A Orszag. Numerical solution of problems in unbounded regions: coordinate transforms. *Journal of Computational Physics*, 25(3):273–295, 1977.
- [77] John P Boyd. *Chebyshev and Fourier spectral methods*. Courier Corporation, 2001.
- [78] Jie Shen, Tao Tang, and Li-Lian Wang. *Spectral Methods: Algorithms, Analysis and Applications*, volume 41 of *Springer Series in Computational Mathematics*. Springer Berlin Heidelberg, Berlin, Heidelberg, 2011.
- [79] Anil Zenginoğlu. Hyperboloidal layers for hyperbolic equations on unbounded domains. *Journal of Computational Physics*, 230(6):2286–2302, 2011.
- [80] Sebastiano Bernuzzi, Alessandro Nagar, and Anil Zenginoğlu. Binary black hole coalescence in the large-mass-ratio limit: the hyperboloidal layer method and waveforms at null infinity. *Physical Review D*, 84(8):084026, 2011.
- [81] David Hilditch, Enno Harms, Marcus Bugner, Hannes Rüter, and Bernd Brügmann. The evolution of hyperboloidal data with the dual foliation formalism: mathematical analysis and wave equation tests. *Classical and Quantum Gravity*, 35(5):055003, 2018.
- [82] Maulik K Parikh. New coordinates for de Sitter space and de Sitter radiation. *Physics Letters B*, 546(3):189–195, October 2002.
- [83] Piotr Bizoń and Patryk Mach. Global dynamics of a Yang-Mills field on an asymptotically hyperbolic space. *Transactions of the American Mathematical Society*, 369(3):2029–2048, 2017.